Photonic crystal MEMS emitter for chemical gas sensing

Nanxi Li[a], Qin Chao[a], Zhonghua Gu[a], Shiwei Song[a], Yanyan Zhou[a], Shaonan Zheng[a], Linfang Xu[a], Yun Da Chua[b], Qingxin Zhang[a], Hong Cai[a], Daohua Zhang[b], Qi Jie Wang[b] and Lennon Lee[a*]

[a]Institute of Microelectronics, A*STAR (Agency for Science, Technology and Research), 2 Fusionopolis Way, #08-02 Innovis Tower, Singapore 138634
[b]School of Electrical and Electronic Engineering, Nanyang Technological University, 50 Nanyang Ave, 639798, Singapore

ABSTRACT

A thermal emitter fabricated on complementary metal-oxide-semiconductor (CMOS)-compatible facilities is a key component for low-cost mid-infrared gas sensing. While conventional thermal emitters have broad spectrum and wide emission angle, which limit the sensing performance. In this work, a microelectromechanical system (MEMS)-based thermal emitter with photonic crystal has been designed and fabricated using CMOS-compatible technology. The photonic crystal enables the emission wavelength selectivity within mid-infrared regime. By engineering photonic crystal dimension, the emission enhancement wavelength can be matched to the fingerprint wavelength of chemical gas for efficient chemical gas sensing purpose.

Keywords: MEMS, thermal emitter, photonic crystal, chemical sensor.

1. INTRODUCTION

Chemical gas sensors have wide applications in industrial process control, in-door air quality check and environmental monitoring. Mid-infrared (mid-IR) optical sensors are commonly used for chemical gas sensing since most chemicals have their fingerprints in this wavelength regime [1]. Also, the optical sensor has advantages of fast response, high long-term lifetime and operational stability. A thermal emitter fabricated on complementary metal-oxide-semiconductor (CMOS)-compatible facilities is a key component for low-cost, compact mid-IR gas sensing [2]. Meanwhile, microelectromechanical system (MEMS)-based thermal emitters have proven to be an effective solution for gas sensing contributed by its compact size [3], fast response time [4] and low power consumption [5]. Furthermore, its fabrication is compatible with the CMOS fabrication facilities [3,6]. Conventional MEMS-based thermal emitters are emitting broadly and also in all angles [4,7,8], which limit their effectiveness when used in a system for high sensing performance in terms of sensitivity and limit of detection (LOD). A thermal emitter with tailorable emission wavelength will be attractive for chemical gas sensors with improved sensing performance. Different approaches have been applied to achieve the expected emission wavelength selectivity, including metamaterials [9], photonic crystals [10,11], and plasmonic-based filters [12,13]. These approaches in combination with MEMS-based thermal emitter to achieve tailorable emission wavelength are in favor for further development.

In this work, we demonstrate a MEMS-based thermal emitter with photonic crystal to tailor the emission wavelength, which has been designed and fabricated using CMOS-compatible technology. The doped silicon layer is used as a resistance-based heater for thermal emission. The honeycomb-structured photonic crystal, which is formed by etching holes on doped silicon layer, enables the emission wavelength selectivity within the mid-IR regime. By engineering the photonic crystal dimension including hole diameter and period, the emission enhancement wavelength can be designed to match with the fingerprint wavelength of the chemical gas for efficient sensing purpose. The fabrication process of the designed MEMS-based thermal emitter has been presented. Its preliminary characterization results are also included in this conference paper. For the proof-of-concept demonstration, the photonic crystal has been designed with resonance wavelength around 4.2 μm, and applied for CO_2 gas sensing.

* lennon-lee@ime.a-star.edu.sg; phone 65 67705413; a-star.edu.sg/ime

2. MEMS EMITTER DESIGN AND FABRICATION

2.1 Emitter Design

The schematic of photonic crystal thermal emitter is shown in Fig. 1(a) below. The emitter chip has a compact size of 400 μm length, and 100 μm width. N+ doped Si is used as resistor for thermal emission. The emission area is patterned with holes to form the photonic crystal for emission wavelength tailoring. The oxide layer below the emission area is etched away to form a suspended membrane for heat isolation. The length of the emission area is varied from 70 to 110 μm. The photonic crystal structure is formed by honeycomb air holes in doped silicon slab, with schematic shown in Fig. 1(b). The air hole diameter and lattice period are variations in design, with variation range of 3.29-4.33 μm, and 0.9-1.8 μm, respectively. The design goal is to achieve emission enhancement around 4.2 μm, where the absorption peak of CO_2 gas is located.

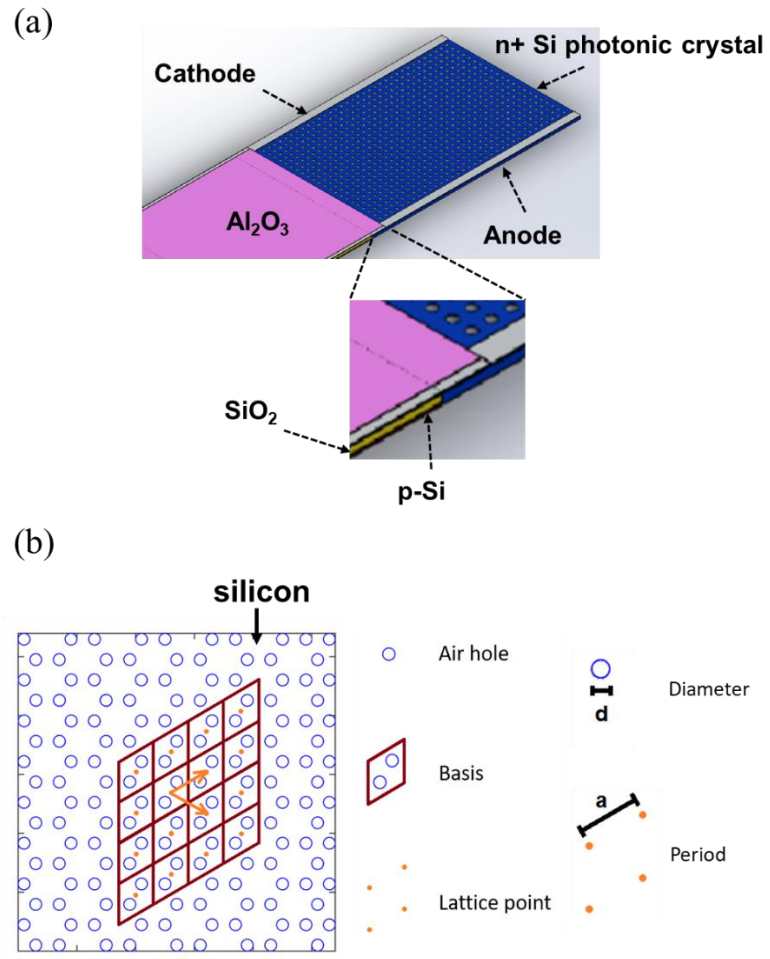

Figure 1. (a) Schematic of photonic crystal MEMS emitter design. Emission area is formed by N-doped Si layer suspended for thermal isolation. (b) Schematic of photonic crystal design, with air holes patterned in doped Si layer. Air holes form honeycomb photonic crystal structure with hole diameter and period as variation.

2.2 Wafer Fabrication

The fabrication process is illustrated in Fig. 2(a). It starts from 8-inch silicon-on-insulator (SOI) wafer. Low-pressure chemical vapor deposition (LPCVD) SiN is deposited and patterned as LOCOS (LOCal Oxidation of Silicon) hard mask, as shown in step I. The process is followed by thermal oxidation, and H_3PO_4 wet etching removal of LPCVD SiN to form thick thermal oxide heat isolation and electrical isolation zone, as shown in step II. This is to prevent the heat from the emission zone impacting other working zones, and also to prevent micro ampere level current leakage. Medium current

N+ implantation is then conducted on Si layer to make it electrically conductive as thermal emitter, as shown in step II. The aluminum contact is then sputtered and patterned on top (step III). Then an Al_2O_3 layer with thickness of 60 nm is deposited on top as protection for oxide below (step IV). Part of the Al_2O_3 layer is then removed through dry etching, to open up the window on aluminum bond pad and on emitter area (step V). A 100 nm oxide layer is re-deposited on top as cladding oxide, to cover aluminum bond pad, meanwhile to work as later silicon dry etching hard mask (step VI). Then the doped Si is patterned to form the emission area. A window has been opened (right hand side) by oxide dry etching followed with silicon dry etching, meanwhile, small holes are patterned by the same layer through dry etching (step VII). In the last step, part of the oxide is etched away by oxide isotropic etching using vapor hydrogen fluoride (HF) to form the suspended membrane for MEMS thermal emitter. Cladding oxide has also been removed through the same etching process to expose the aluminum bond pad and emission zone (step VIII). The scanning electron microscopy (SEM) image of the fabricated MEMS emitter is shown in Fig. 2(b). Fig. 2(c) shows the optical image of the emitter before last etching step. In order to visualize the cross section of the device, focused ion beam (FIB) has been used to cut the emitter, whose location is illustrated by red mark in Fig. 2(c). The transmission electron microscopy (TEM) image is presented in Fig. 2(d).

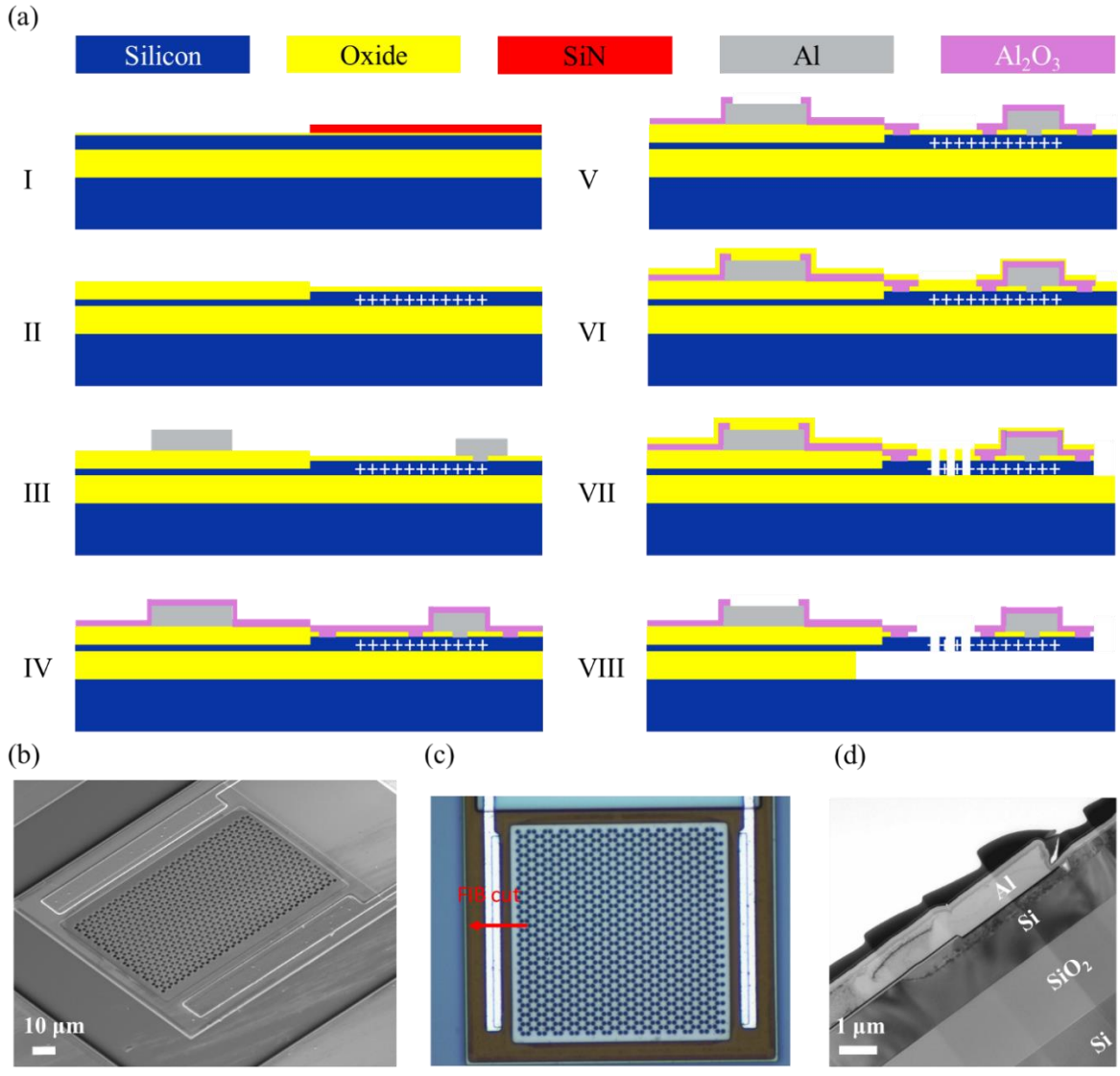

Figure 2. (a) Fabrication process flow of photonic crystal MEMS thermal emitter. (b) Scanning electron microscopy (SEM) image of fabricated MEMS emitter. (c) Optical image of emission area with photonic crystal before final oxide etching step. The focused ion beam cut location is marked in red. (d) Transmission electron microscopy (TEM) image of MEMS emitter before final oxide etching step.

3. EMITTER CHARACTERIZATION

3.1 Time Domain Response

After wafer fabrication and dicing, the emitter chip is packaged on a TO can with wire bonding for further characterization. The time domain response characterization setup and the optical image of the packaged thermal emitter on TO can are shown in Fig. 3(a) and 3(b), respectively. The signal generator cascaded with a unity gain amplifier is used to provide square-wave modulation signal to drive the MEMS thermal emitter. The packaged emitter is mounted within a compound parabolic concentrator, as indicated as device under test (DUT) in Fig. 3(a). The emission light is detected by a photodetector (Thorlabs PDA20H-EC), with detection wavelength range from 1.5 μm to 4.8 μm. The MEMS emitters without and with photonic crystal are tested for comparison, under the same driving voltage and with the same emission area. The captured time responses by oscilloscope for emitters without and with photonic crystal are shown in Fig. 3(c) and 3(d), respectively. The modulation voltage signal has square wave shape, with 500 Hz frequency, 5V peak-to-peak value, and 0.5 duty cycle. For emitter without photonic crystal, the response can be barely observed, as shown in red line in Fig. 3(c). In comparison, for emitter with photonic crystal, the response can be clearly observed, as shown in red line in Fig. 3(d). The rise and fall time can be obtained as 127 μs and 46 μs, respectively. Such comparison indicates the emission enhancement by photonic crystal within the testing wavelength range from 1.5 μm to 4.8 μm. This is further verified by the emission spectrum characterization in later sub-section.

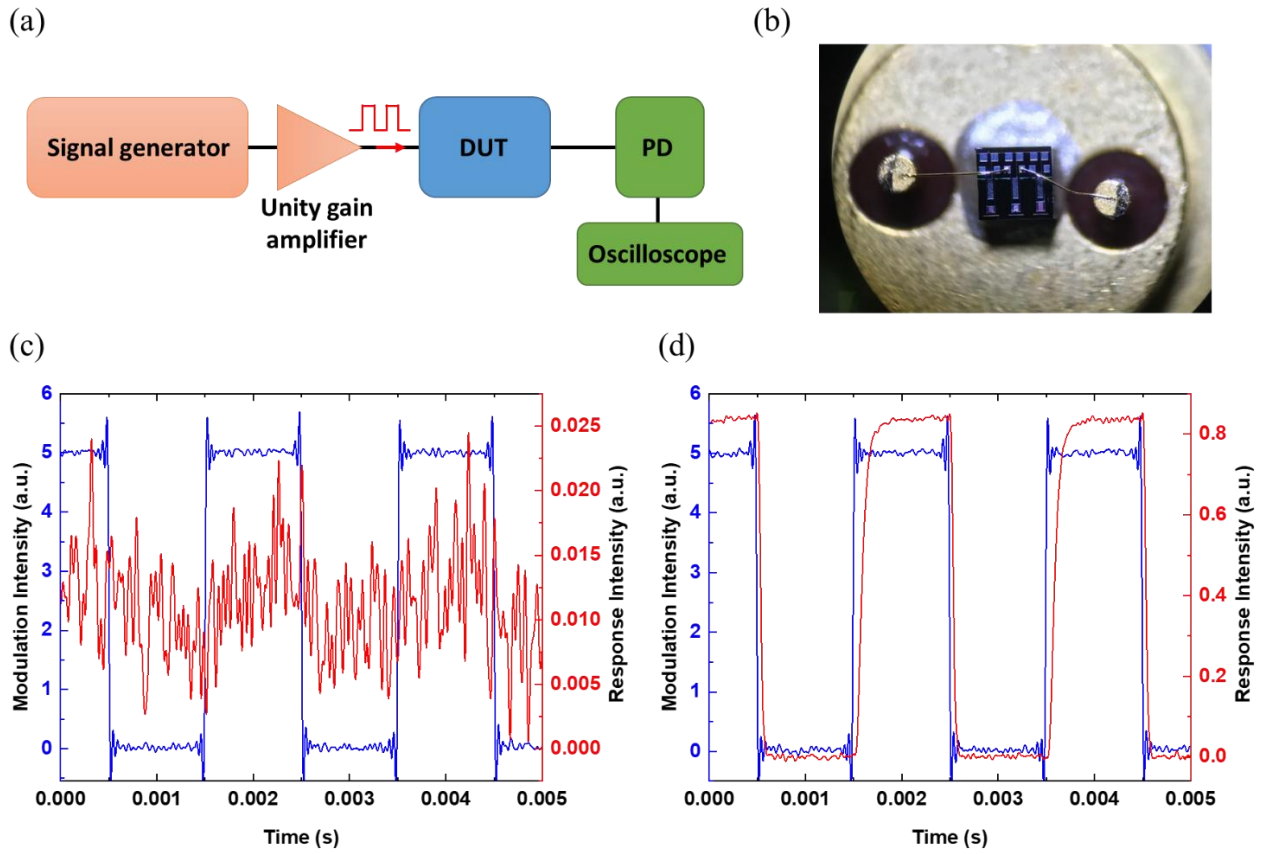

Figure 3. (a) Time domain characterization setup. DUT: device under test. PD: photodetector. Signal generator cascaded with unity gain amplifier is used to drive the DUT. PD (Thorlabs PDA20H-EC) with detection wavelength range from 1.5 μm to 4.8 μm cascaded with oscilloscope is used for capturing the time domain response. (b) Optical image of the packaged emitter on TO can with wire bonding. (c) Time domain modulation signal and response for emitter without photonic crystal. (d) Time domain modulation signal and response for emitter with photonic crystal.

3.2 Emission spectrum

The emission spectrum of emitters with and without photonic crystal are captured using the characterization setup shown in Fig. 4(a). Differentiating from the earlier setup in Fig. 3(a), Fourier-transform infrared (FTIR) spectrometer (Bruker VERTEX 70 series) has been used to capture the emission spectrum. Also, the DUT is driven by DC driving voltage for FTIR measurement. The emission spectrum comparison between the emitter with and without photonic crystal is made in Fig. 4(b). The emitters are driven by the same bias voltage, and the peak intensity are normalized to 1 for comparison. It can be observed that the emitter with photonic crystal has more emission intensity around 5 μm wavelength, but less emission intensity around 12.5 μm compared with the emitter without photonic crystal. Fig. 4(c) shows the zoom-in view of Fig. 4(b) between 4 μm and 7 μm. The intensity ratio between the emitter with and without photonic crystal is plotted in Fig. 4(d). The emission spectrum in Fig. 4 verifies the emission enhancement around 4 μm by photonic crystal observed in Fig. 3. An additional note worth mentioning is that the comparisons between emitter with and without photonic crystal in Fig. 3 and Fig. 4 are under the same bias voltage. The resistance of emitter with photonic crystal (around 70 Ω) is relatively higher than the emitter without photonic crystal (around 50 Ω), since it has etched holes. The difference or enhancement will be more significant if these emitters are compared under the same driving power.

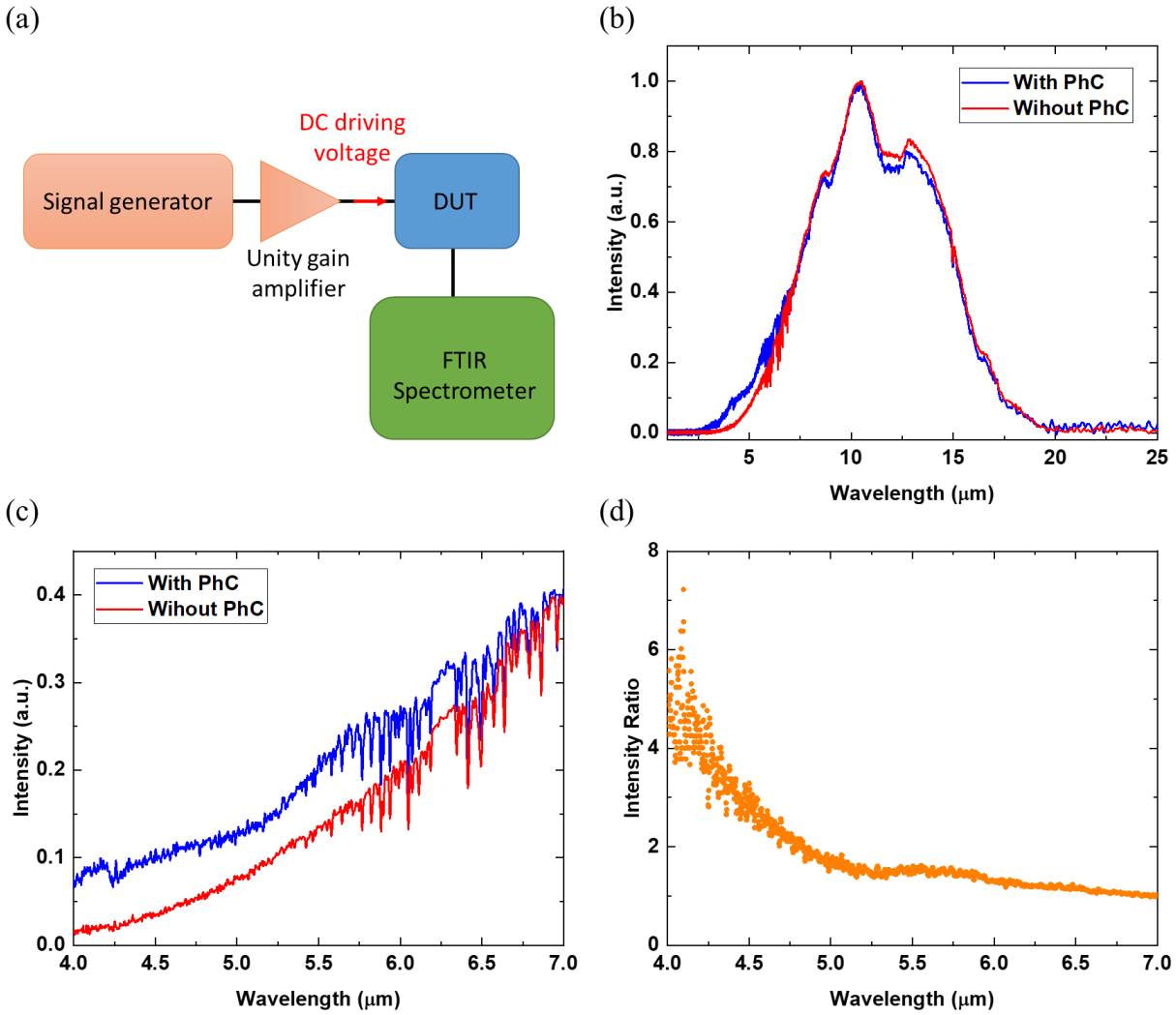

Figure 4. (a) MEMS emitter spectrum characterization setup. FTIR: Fourier-transform infrared. (b) Normalized spectrum of emitters with and without photonic crystal under same bias voltage, captured by FTIR spectrometer. PhC: Photonic crystal. (c) Zoom-in view of (b), showing more significant emission between wavelength from 4 μm to 7 μm contributed by photonic crystal. (d) Intensity ratio calculated based on (c) between wavelength from 4 μm to 7 μm.

4. APPLICATION IN OPTICAL GAS SENSING

The photonic crystal MEMS emitter has been used for CO_2 gas sensing as a proof-of-concept functionality demonstration. The optical image of the home-made gas testing chamber with control circuit board on top is shown in Fig. 5(a). The MEMS emitter is mounted on the left side, and a photodetector with a spectrum filter is placed on the right side of the chamber. The CO_2 gas is mixed with N_2 gas. The CO_2 gas concentration is controlled and varied by a mass flow controller. The voltages at the photodetector after amplification are recorded. Fig. 5(b) presents the voltage data after smoothing process. The CO_2 gas concentrations are varied from 200 to 500 ppm with 100 ppm increasing step, and from 500 to 5000 ppm with 500 ppm increasing step. The 5000 ppm is then repeated for three times, and the voltage is able to come back to the same level at each time.

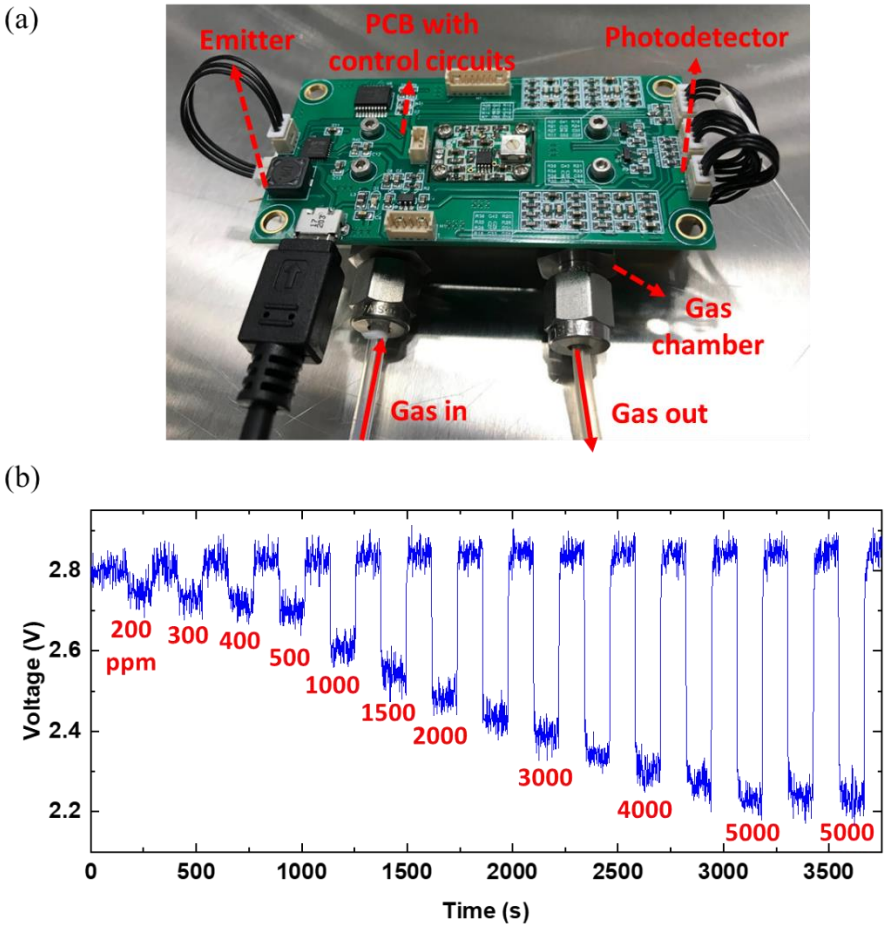

Figure 5. (a) Optical image of home-made CO_2 gas sensing chamber with emitter mounted on left side, photodetector with spectrum filter mounted on right side, control circuits integrated on top. (b) Amplified voltage of photodetector with respect to time under different CO_2 gas concentration (after data smoothing process).

5. CONCLUSION

In summary, photonic crystal MEMS thermal emitter has been designed, fabricated, and characterized in this work. The photonic crystal follows a honeycomb structure, with dimension engineered to improve the emission around 4.2 μm wavelength. The wafer-scale fabrication process flow has been included, which is compatible with CMOS fabrication infrastructure. The emitter with and without photonic crystal are compared in characterization. The time domain response indicates more significant emission around 4.2 μm contributed by the photonic crystal. This is further verified by spectrum measurement result. At last, the emitter with photonic crystal is applied for CO_2 gas sensing as a proof-of-concept functionality demonstration.

ACKNOWLEDGEMENTS

This work is supported by Agency for Science, Technology and Research (IAF-PP A1789a0024 and IAF-PP A19B3a0008) and Singapore National Research Foundation Competitive Research Program (NRF-CRP18-2017-02).

REFERENCES

[1] J. Hodgkinson and R. P. Tatam, "Optical gas sensing: a review," Meas. Sci. Technol. **24**(1), 012004 (2012).
[2] N. Li, H. Yuan, L. Xu, J. Tao, D. K. T. Ng, L. Y. T. Lee, D. D. Cheam, Y. Zeng, B. Qiang, Q. Wang, H. Cai, N. Singh, and D. Zhao, "Radiation Enhancement by Graphene Oxide on Microelectromechanical System Emitters for Highly Selective Gas Sensing," ACS Sens. **4**(10), 2746–2753 (2019).
[3] S. Z. Ali, A. De Luca, R. Hopper, S. Boual, J. Gardner, and F. Udrea, "A Low-Power, Low-Cost Infra-Red Emitter in CMOS Technology," IEEE Sens. J. **15**(12), 6775–6782 (2015).
[4] K.-N. Lee, D.-S. Lee, S.-W. Jung, Y.-H. Jang, Y.-K. Kim, and W.-K. Seong, "A high-temperature MEMS heater using suspended silicon structures," J. Micromech. Microeng. **19**(11), 115011 (2009).
[5] P. Barritault, M. Brun, S. Gidon, and S. Nicoletti, "Mid-IR source based on a free-standing microhotplate for autonomous CO2 sensing in indoor applications," Sens. Actuator A Phys. **172**(2), 379–385 (2011).
[6] P. K. Guha, S. Z. Ali, C. C. C. Lee, F. Udrea, W. I. Milne, T. Iwaki, J. A. Covington, and J. W. Gardner, "Novel design and characterisation of SOI CMOS micro-hotplates for high temperature gas sensors," Sens. Actuators B Chem. **127**(1), 260–266 (2007).
[7] J. Hildenbrand, J. Korvink, J. Wollenstein, C. Peter, A. Kurzinger, F. Naumann, M. Ebert, and F. Lamprecht, "Micromachined Mid-Infrared Emitter for Fast Transient Temperature Operation for Optical Gas Sensing Systems," IEEE Sens. J. **10**(2), 353–362 (2010).
[8] S. Z. Ali, F. Udrea, W. I. Milne, and J. W. Gardner, "Tungsten-Based SOI Microhotplates for Smart Gas Sensors," J. of Microelectromech. S. **17**(6), 1408–1417 (2008).
[9] A. Lochbaum, Y. Fedoryshyn, A. Dorodnyy, U. Koch, C. Hafner, and J. Leuthold, "On-Chip Narrowband Thermal Emitter for Mid-IR Optical Gas Sensing," ACS Photonics **4**(6), 1371–1380 (2017).
[10] M. U. Pralle, N. Moelders, M. P. McNeal, I. Puscasu, A. C. Greenwald, J. T. Daly, E. A. Johnson, T. George, D. S. Choi, I. El-Kady, and R. Biswas, "Photonic crystal enhanced narrow-band infrared emitters," Appl. Phys. Lett. **81**(25), 4685–4687 (2002).
[11] B. J. O'Regan, Y. Wang, and T. F. Krauss, "Silicon photonic crystal thermal emitter at near-infrared wavelengths," Sci. Rep. **5**(1), 13415 (2015).
[12] A. Pusch, A. De Luca, S. S. Oh, S. Wuestner, T. Roschuk, Y. Chen, S. Boual, Z. Ali, C. C. Phillips, M. Hong, S. A. Maier, F. Udrea, R. H. Hopper, and O. Hess, "A highly efficient CMOS nanoplasmonic crystal enhanced slow-wave thermal emitter improves infrared gas-sensing devices," Sci. Rep. **5**(1), 17451 (2015).
[13] J. Park, J.-H. Kang, X. Liu, S. J. Maddox, K. Tang, P. C. McIntyre, S. R. Bank, and M. L. Brongersma, "Dynamic thermal emission control with InAs-based plasmonic metasurfaces," Sci. Adv. **4**(12), eaat3163 (2018).